Colloids and Surfaces A: Physicochem. Eng. Aspects 396 (2012) 346–351

Contents lists available at SciVerse ScienceDirect

Colloids and Surfaces A: Physicochemical and Engineering Aspects

journal homepage: www.elsevier.com/locate/colsurfa

Short communication

β-$ZnMoO_4$ microcrystals synthesized by the surfactant-assisted hydrothermal method: Growth process and photoluminescence properties

L.S. Cavalcante[a,*], J.C. Sczancoski[a], M. Siu Li[b], E. Longo[a], J.A. Varela[a]

[a] INCTMN – Universidade Estadual Paulista, P.O. Box 355, 14801-907 Araraquara, SP, Brazil
[b] IFSC, Universidade de São Paulo, P.O. Box 369, 13560 970, São Carlos, SP, Brazil

ARTICLE INFO

Article history:
Received 28 August 2011
Received in revised form 17 October 2011
Accepted 7 December 2011
Available online 16 December 2011

Keywords:
β-$ZnMoO_4$
Crystal growth
Surfactants
Photoluminescence

ABSTRACT

In this communication, we investigate the effect of different surfactants: cetyltrimethylammonium bromide (CTAB), sodium dodecyl sulfate (SDS) and polyvinylpyrrolidone (PVP-K40) on the growth process of zinc molybdate (β-$ZnMoO_4$) microcrystals synthesized under hydrothermal conditions at 140 °C for 8 h. These microcrystals were characterized by X-ray diffraction (XRD), field emission scanning electron microscopy (FE-SEM), and photoluminescence (PL) measurements. XRD patterns proved that these crystals are monophasic and present a wolframite-type monoclinic structure. FE-SEM images revealed that the surfactants modified the crystal shapes, suggesting the occurrence of distinct crystal growth processes. The CTAB cationic surfactant promotes the hindrance of small nuclei that leads to the formation of rectangle-like crystals, SDS anionic surfactant induces a growth of irregular hexagons with several porous due to considerable size effect of counter-ions on the crystal facets, PVP-K40 non-ionic surfactant allows a reduction in size and thickness of plate-like crystals, while without surfactants have the formation of irregular plate-like crystals. Finally, the PL properties of β-$ZnMoO_4$ microcrystals were explained by means of different shape/size, surface defects and order-disorder into lattice.

1. Introduction

Zinc molybdate ($ZnMoO_4$) is an inorganic material found in nature with two different types of crystalline phase: α-triclinic and β-monoclinic. In the α-$ZnMoO_4$ triclinic structure, all zinc (Zn) atoms are bonded to six oxygens (O) atoms, forming the distorted octahedral [ZnO_6] clusters. The molybdenum (Mo) atoms are coordinated to four O atoms, resulting in the tetrahedral [MoO_4] clusters [1,2]. On the other hand, the β-$ZnMoO_4$ monoclinic structure has both Zn and Mo atoms bonded to six O atoms, which promote the origin of distorted octahedral [ZnO_6]/[MoO_6] clusters, respectively [3].

In the last years, α- and β-$ZnMoO_4$ crystals have been widely studied because of its relevance for technological applications in photoluminescence (PL) field [4–6], red/green phosphors for light-emitting diode [7–9], photocatalytic degradation of auramine O [10], cryogenic/bolometric scintillating detectors [11,12], anticorrosive paints [13], cathode electrodes in rechargeable lithium batteries [14], and humidity sensors [15]. Traditionally, the α- and β-$ZnMoO_4$ crystals have been prepared by oxide mixture or solid state reaction [16–18], precipitation/calcination [19,20], and citrate complex precursor methods [21]. However, these preparation routes require high temperatures, long processing times and use of organic precursors/solvents. Recently, the conventional hydrothermal (HT) and microwave-assisted hydrothermal methods have been well-employed in the preparation, growth and morphological control of different oxide materials, such as: molybdates, tungstates, titanates and zirconates [22–29]. In particular, the main advantage of the HT is the ability to obtain pure oxides at low temperature conditions (140–180 °C). Moreover, capping agents, templates and/or surfactants can be added in the chemical solution to be submitted to the hydrothermal treatment in order to control the crystal shapes and sizes (nano-, meso- or micro-scale) [30–33].

Therefore, in this communication, we report on the effect of different surfactants, such as: cetyltrimethylammonium bromide (CTAB), sodium dodecyl sulfate (SDS), polyvinylpyrrolidone (PVP-K40), and without surfactant on the growth process and PL properties at room temperature of β-$ZnMoO_4$ microcrystals synthesized by the HT method at 140 °C for 8 h.

2. Experimental details

2.1. Hydrothermal synthesis of β-$ZnMoO_4$ microcrystals

β-$ZnMoO_4$ microcrystals were prepared by the HT method without and with the presence of surfactants, such as: CTAB-[$(C_{16}H_{33})N(CH_3)_3Br$] (99% purity, Sigma–Aldrich),

* Corresponding author. Tel.: +55 16 3361 52 15; fax: +55 16 3361 82 14.
E-mail address: laeciosc@bol.com.br (L.S. Cavalcante).

0927-7757/$ – see front matter © 2011 Elsevier B.V. All rights reserved.
doi:10.1016/j.colsurfa.2011.12.021

SDS-$C_{12}H_{25}SO_4Na$ (99% purity, Sigma–Aldrich), and PVP-K40-$(C_6H_9NO)_n$ (n = 40) (99% purity, Sigma–Aldrich). The typical experimental procedure for the preparation of these microcrystals is described as follows: 2.5×10^{-3} moles of molybdate (VI) sodium dihydrate [$Na_2MoO_4{\cdot}2H_2O$] (99.5% purity, Sigma–Aldrich) and 2.5×10^{-3} moles of zinc (II) nitrate hexahydrate [$Zn(NO_3)_2{\cdot}6H_2O$] (99% purity, Sigma–Aldrich) were separately dissolved with deionized water contained in two plastic tubes (50 mL in each) (Falcon – capacity of 50 mL). These solutions were simultaneously mixed inside a stainless autoclave and then kept under constant stirring. The synthesis using the CTAB, SDS or PVP-K40 is very similar to those performed only in H_2O. The main difference is that after individual dissolution of $Na_2MoO_4{\cdot}2H_2O$ and $Zn(NO_3)_2{\cdot}6H_2O$ precursors in each plastic tube, it was added 0.5 g of the chosen surfactant in each of them. The HT synthesis was performed in stainless autoclave at 140 °C for 8 h under constant pressure of 4.5 bar. These experimental conditions were favorable to promotes the stoichiometric chemical reactions between the Zn^{2+} and MoO_4^{2-} ions, which are responsible for the formation of the crystalline β-$ZnMoO_4$ microcrystals, as shown in the following Eqs. (1)–(3):

After dissolution of the salts at room temperature:

$$Na_2MoO_4 \cdot 2H_2O_{(s)} \xrightarrow{H_2O(25^{o}C)} 2Na^{+}_{(aq)} + MoO^{2-}_{4(aq)} + 2H_2O \quad (1)$$

$$Zn(NO_3)_2 \cdot 6H_2O_{(s)} \xrightarrow{H_2O(25^{o}C)} Zn^{2+}_{(aq)} + 2NO^{-}_{3(aq)} + 6H_2O \quad (2)$$

After HT processing:

$$2Na^{+}_{(aq)} + MoO^{2-}_{4(aq)} + 2H_2O + Zn^{2+}_{(aq)} + 2NO^{-}_{3(aq)} + 6H_2O \xrightarrow{140\ ^{o}C/8\,h} \beta\text{-}ZnMoO_{4(s)} + 2Na^{+}_{(aq)} + 2NO^{-}_{3(aq)} + 8H_2O \quad (3)$$

Completed the HT processing, the stainless autoclave was naturally cooled to room temperature. The resulting suspensions were washed several times with deionized water and acetone to remove the residual ions (for example, Na^+/Br^-) and organic compounds. Finally, the crystalline β-$ZnMoO_4$ precipitated (light-gray color) were collected and dried on a hot plate at 65 °C for 10 h.

2.2. Characterizations

These microcrystals were structurally characterized by X-ray diffraction (XRD) using a DMax-2500PC diffractometer (Rigaku, Japan) with Cu-Kα radiation (λ = 1.5406 Å) in the 2θ range from 10° to 72°, using a scanning rate of 0.02°/min and total exposure time of 15 min. The shape and size of these β-$ZnMoO_4$ microcrystals were observed with a field emission scanning electron microscopy (FE-SEM) model Inspect F50, FEI Company, Hillsboro (USA) operated at 5 kV. The PL measurements were performed through a Monospec 27 monochromator (Thermal Jarrel Ash, USA) coupled to a R446 photomultiplier (Hamamatsu Photonics, Japan). A krypton ion laser (Coherent Innova 90K, USA) (λ = 350 nm) was used as excitation source, keeping its maximum output power at 500 mW. The laser beam was passed through an optical chopper and its maximum power on the sample was kept at 40 mW. The PL measurements were performed at room temperature.

3. Results and discussion

3.1. XRD analyses

Fig. 1(a–d) shows the XRD patterns of β-$ZnMoO_4$ microcrystals synthesized without and with differents surfactants: (CTAB, PVP-K40 and SDS) by the HT method at 140 °C for 8 h.

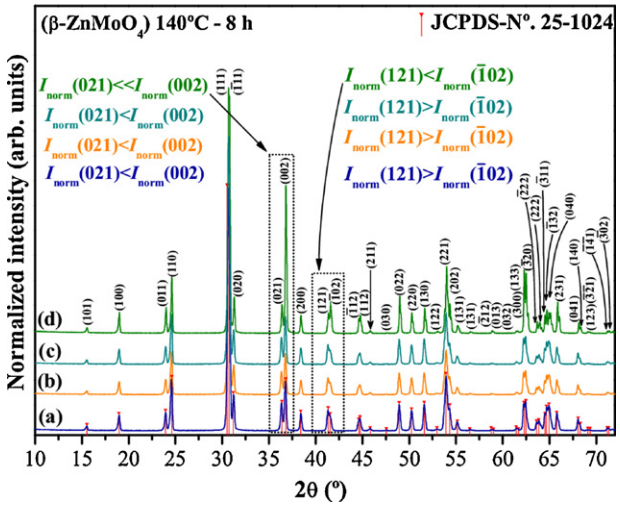

Fig. 1. XRD patterns of β-$ZnMoO_4$ microcrystals synthesized in HT system at 140 °C for 8 h: (a) H_2O – without surfactant, and with different surfactants: (b) CTAB, (c) PVP-K40, and (d) SDS, respectively.

In these XRD patterns, all diffraction peaks were well-indexed to the wolframite-type monoclinic structure with space group ($P2/c$) and point group symmetry (C_{2h}^4), as described in the respective Joint Committee on Powder Diffraction Standards (JCPDS) card No. 25-1024 [34] (Fig. 1(a–d)). In a first analysis, the narrow and intense diffraction peaks suggest that the β-$ZnMoO_4$ phase is constituted of large crystals with considerable degree of structural order at long-range. In Fig. 1(d) was noted that the microcrystals prepared with SDS (anionic surfactant) exhibited a slightly effect of crystallographic orientation in relation to β-$ZnMoO_4$ microcrystals (Fig. 1(a–c)). This phenomenon was more evidenced by means of the diffraction peaks associated to the (0 2 1)/(0 0 2) and (1 2 1)/($\bar{1}$ 0 2) plans, specially when compared to the standard diffraction pattern (JCPDS card No. 25-1024) and with the other microcrystals. Based on this information, it was observed that the [I_{norm}(0 2 1) ≪ I_{norm}(0 0 2) plan] and [I_{norm}(1 2 1) < I_{norm}($\bar{1}$ 0 2)] plan, respectively.

3.2. FE-SEM analyses

Fig. 2(a–h) illustrates the FE-SEM images of β-$ZnMoO_4$ microcrystals synthesized without and with differents surfactants: (CTAB, PVP-K40 and SDS) by the HT method at 140 °C for 8 h, respectively.

The low and high-magnification FE-SEM images in Fig. 2(a and b) showed the presence of agglomerated regions composed of several irregular plate-like β-$ZnMoO_4$ microcrystals for the HT processing performed only in H_2O. The influence of surfactants was initially verified in the synthesis employing the CTAB (cationic surfactant) caused a drastic morphological modification from plate- to rectangle-like β-$ZnMoO_4$ microcrystals (Fig. 2(c and d)). The chemical strategy employing the PVP-K40 as non-ionic or polymeric surfactant promotes the creation of surface roughness and reduced the thickness and size of these plates (Fig. 2(e and f)). On the other hand, the SDS (anionic surfactant) modified the crystal shape to irregular hexagons and stimulate the formation of small surface defects (Fig. 2(g and h)).

3.3. Growth mechanism of β-$ZnMoO_4$ microcrystals

A possible growth mechanism for the microcrystals was proposed to explain in details the effect of different surfactants on the shape and size (Fig. 3(a–j)).

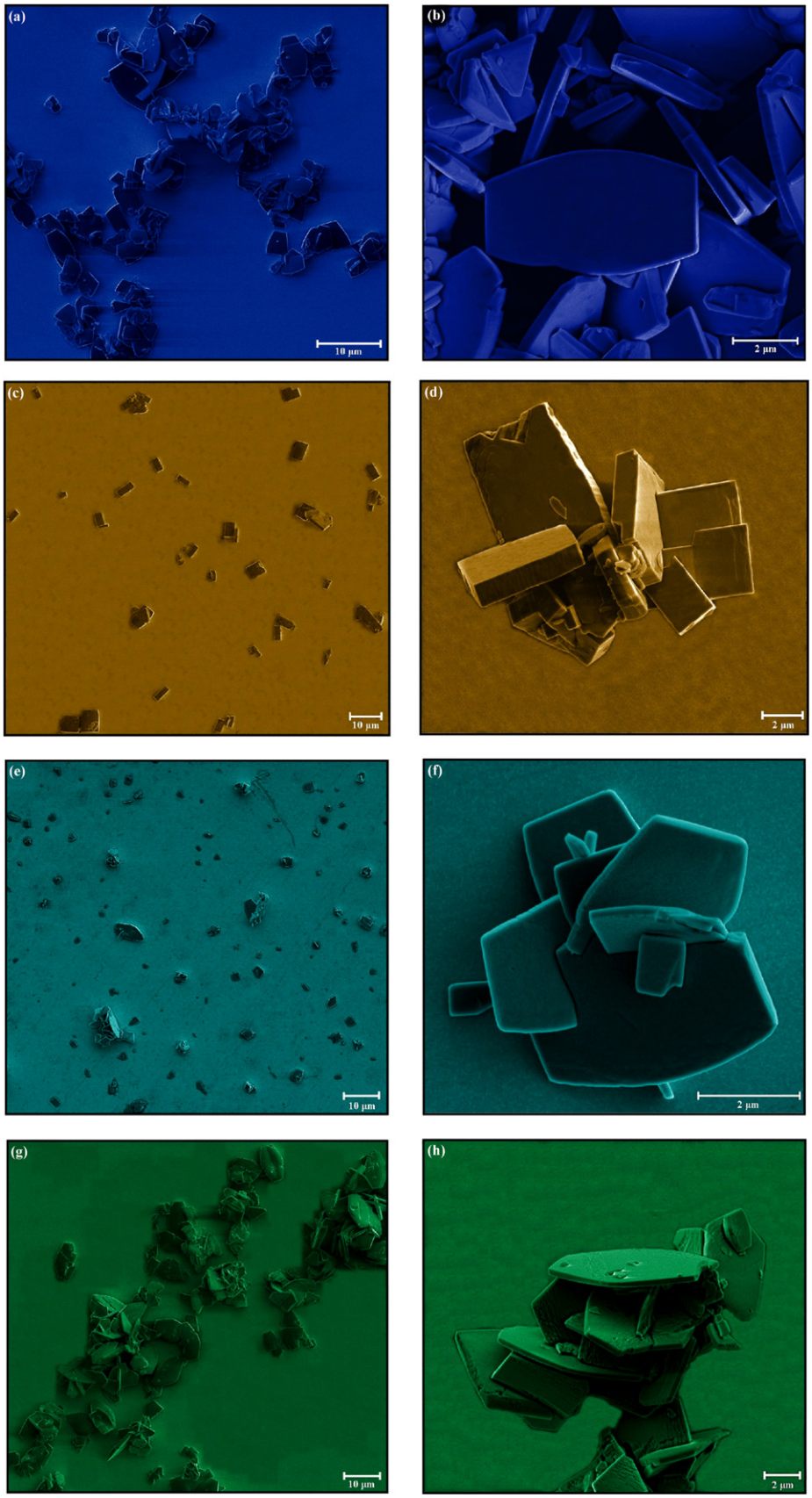

Fig. 2. FE-SEM images of β-$ZnMoO_4$ microcrystals synthesized in HT system at 140 °C for 8 h: (a and b) H_2O – without surfactant, and with different surfactants: (c and d) CTAB, (e and f) PVP-K40, and (g and h) SDS, respectively.

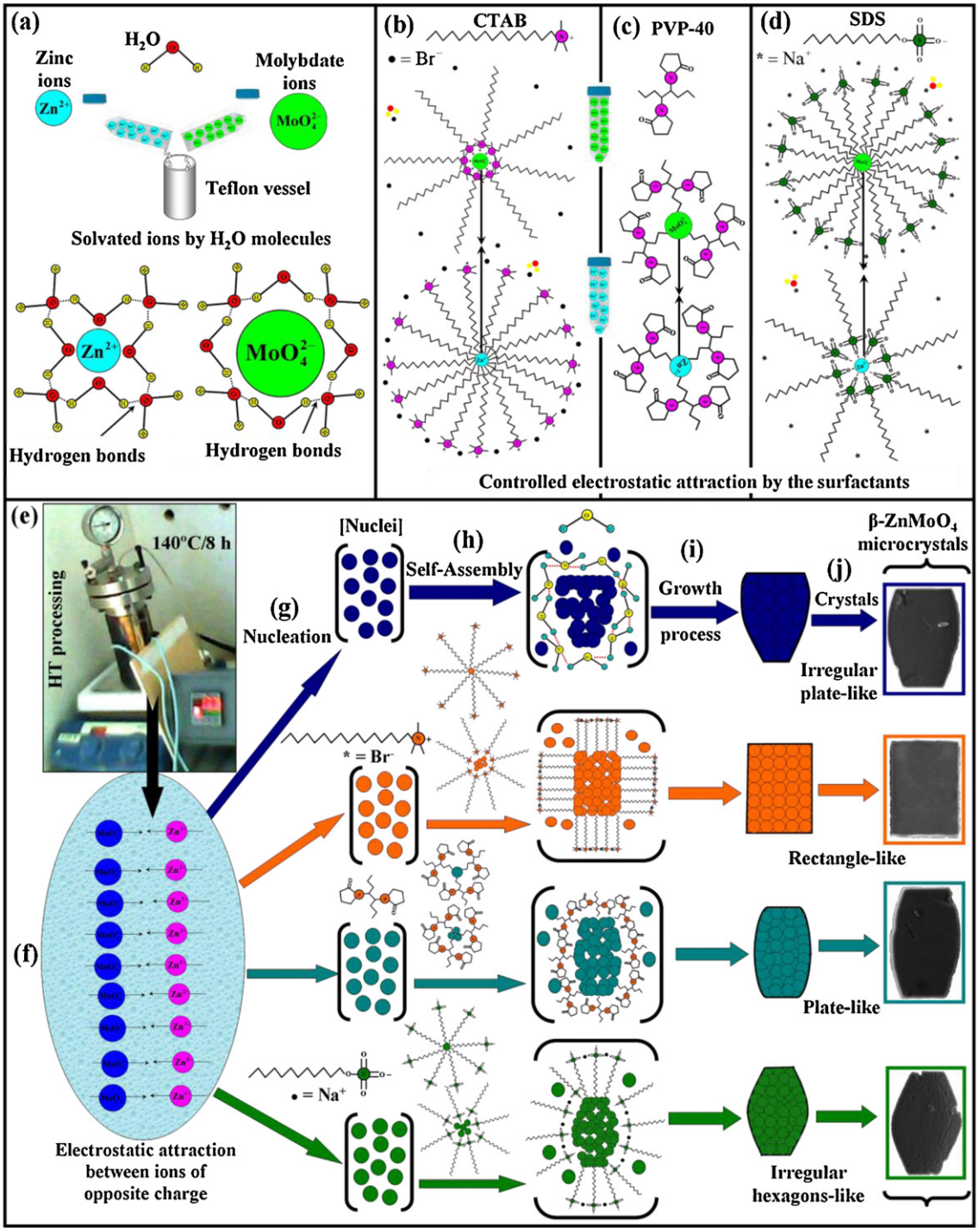

Fig. 3. Schematic illustration of the main stages involved in the growth mechanism of β-$ZnMoO_4$ microcrystals: (a) dissolution of the sais without surfactant (H_2O as solvent) and with different surfactants: (b) CTAB; (c) PVP-40; (d) SDS; (e) hydrothermal reactor; (f) electrostatic interaction between the Zn^{2+} and MoO_4^{2-} ions under HT condition; (g) nucleation and origin of the first clusters or nuclei; (h) self-assembly process of small nanocrystals; (i) crystal growth process, and (j) FE-SEM images of the microcrystals synthesized in HT system at 140 °C for 8 h.

This growth mechanism was based on the FE-SEM micrographs. Firstly in Fig. 3(a), the free energy of solvation related to the H_2O molecules causes a fast dissociation of the chemical salts in solution, so that the Zn^{2+} and MoO_4^{2-} ions are rapidly solvated by these molecules. The partial negative charges belonging to the H_2O molecules electrostatically attract the Zn^{2+} ions, while its partial positive charges interact with the MoO_4^{2-} ions [35]. In the case of CTAB (cationic surfactant) (Fig. 3(b)), its molecule contains a hydrophobic long-chain (tail – apolar) bonded to a positively charged group (head – polar). When the CTAB is solubilized in water, these molecules spontaneously tend to arrange themselves into organized assemblies known as micelles [36]. Besides of this surfactant, it was also used in the chemical synthesis a non-ionic polymer known as PVP-K40. This polymer is easily dissolved in H_2O and it is formed by uncountable *N*-vinylpyrrolidone monomers (Fig. 3(c)). Opposite from CTAB, the SDS is an anionic surfactant with hydrophobic-short chain (apolar) connected to a negative ionic group (head – polar) (Fig. 3(d)). The SDS has the same facility of

forming the micelles in H_2O as far as the CTAB, since that the critical micelle concentration can be achieved.

In principle, during the HT processing performed at 140 °C for 8 h inside the stainless autoclave (Fig. 3(e)), this closed environment provided the thermodynamic conditions to break the aqueous solvation shell, favoring the electrostatic attraction and between both the Zn^{2+} and MoO_4^{2-} ions by the nucleation process with the formation of first β-$ZnMoO_4$(s) precipitates or nuclei (Fig. 3(f and g)). When the H_2O molecules were used as solvent, the hydrogen bonds (highly polar) were able to make two hydrogen atoms (H δ$^+$), belonging to one H_2O molecule, strongly interact with other two neighboring H_2O molecules. In another case also involving the H_2O solution, the oxygen atoms (O δ$^-$) (containing two free electron pairs) of each H_2O molecule have the ability of form the hydrogen bridges or interact with the H atoms bonded to other H_2O molecules [37] (Fig. 3(a)). There are a correct number of hydrogen atoms (H δ$^+$) and lone electron pairs within the liquid system, so that each them can be involved by hydrogen bonds [38]. After formation of the first nuclei, the HT conditions intensify the effective collision frequency involving the anisotropic nanoparticles in suspension, producing a mutual aggregation between them. This self-assembly process can occur in a spontaneous way and/or and hydrothermal conditions (Fig. 3(h)), where several nanocrystals are aggregated in a same or different crystallographic plane which can drive the growth of oriented aggregate, meso- and nanocrystals [39,40]. Theoretically after an effective chock, if the nanoparticles share a common crystallographic orientation, they may remain irreversibly attached (Fig. 3(h)). Moreover, the nanoparticles can be surrounded by H_2O molecules in this suspension, which tend to change or direct the growth of the microcrystals (Fig. 3(i)). After agglomeration process (disordered assemblies), probably occurred the coalescence of nanoparticles followed by Ostwald ripening [41], resulting in the irregular plate-like β-$ZnMoO_4$ microcrystals (Fig. 3(j)). When the CTAB (molecular formula: $C_{19}H_{42}BrN$) was added in the solvent (H_2O), before the chemical precursors ($Na_2MoO_4{\cdot}2H_2O$ and $Zn(NO_3)_2{\cdot}6H_2O$), spontaneously the micelles were formed in this medium. Basically, the ● = Br^- ions remain solvated by the H_2O molecules and bonded to a polar positive head (R—N^+≡), where both are chemically connected to a tail with high molecular weight ($R = C_{19}H_{42}$) (Fig. 3(b)). In fact, the MoO_4^{2-} ions will be trapped or bonded to the polar heads (R—N^+≡), occupying the inside of the micelles. On the other hand, the tails formed by nineteen carbon-long chains of this surfactant prevent the free diffusion of Zn^{2+} ions toward those of MoO_4^{2-} ions [42] (Fig. 3(b)). For a simplified description, the CTAB inhibits or reduces the electrostatic attraction between the opposite charged ions. The HT environment (140 °C for 8 h) favors an ideal thermodynamic condition to disorganize the micelles and induce a controlled interaction of Zn^{2+} and MoO_4^{2-} ions, leading to the formation and growth of nanocrystals (Fig. 3(h)). These nanocrystals self-aggregate forming the rectangle-like β-$ZnMoO_4$ microcrystals (Fig. 3(i and j)). The non-ionic surfactant (PVP-K40) presents a certain degree of viscosity that plays the role to decrease the spontaneous interaction of Zn^{2+} and MoO_4^{2-} ions even under HT conditions (Fig. 3(h)). As a consequence of this process, a slow velocity of formation and aggregation of several nanocrystals takes place in this system, promoting to the origin and growth of thin plates-like β-$ZnMoO_4$ crystals [43] (Fig. 3(i and j)). Finally, in the synthesis with SDS, the dissolution of this anionic surfactant releases (* = Na^+ ions) and negative polar heads (R–SO_3^-) as counter ions [44] (Fig. 3(d)). These negative heads have more ability to bond with the Zn^{2+} ions (Fig. 3(b)). However, the carbon-short chain do not is strong sufficient to avoid the electrostatic interactions of Zn^{2+} ions with those of during the HT processing (Fig. 3(h)). The clusters will grow in a geometric arrangement in order to minimize the surface energy. Thus, the formation and growth of nanocrystals follow a different way of CTAB, where its shapes as well as self-assembly process will result in an organization of irregular hexagon-like β-$ZnMoO_4$ microcrystals (Fig. 3(i and j)).

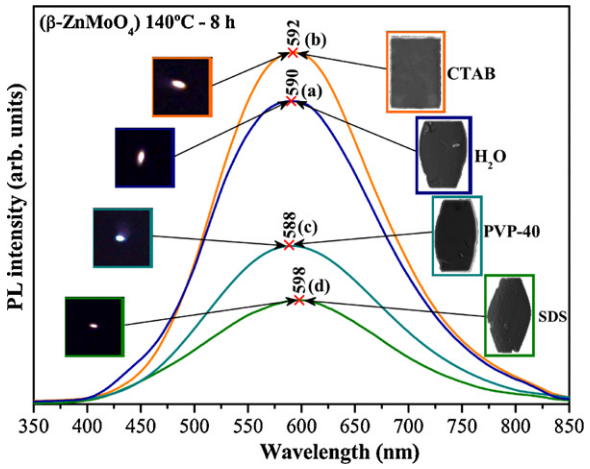

Fig. 4. PL spectra of β-$ZnMoO_4$ microcrystals processed in HT system at 140 °C for 8 h: (a) H_2O – without surfactant, and with different surfactants: (b) CTAB, (c) PVP-40, and (d) SDS. Insets show the digital photos with the PL emissions and FE-SEM images of each individual β-$ZnMoO_4$ microcrystal, respectively.

3.4. PL emission analyses

Fig. 4(a–d) illustrates the PL spectra at room temperature of β-$ZnMoO_4$ microcrystals obtained with different surfactants in the HT system. Insets show the digital photographs of its corresponding PL emissions and FE-SEM images of each individual microcrystal.

According to the literature [4,5], the PL properties of $ZnMoO_4$ crystals are related to self-localized excitons and electronic transitions within the (MoO_4^{2-}) anion molecular complex. However, in our previous works [45,46] on molybdates with scheelite-type structure, we have explained that its PL properties are related to the existence of tetrahedral distorted [MoO_4] clusters within the tetragonal lattice. In this work, for the β-$ZnMoO_4$ microcrystals with a wolframite-type monoclinic structure we assumed only the presence of octahedral distorted [ZnO_6]/[MoO_6] clusters into lattice. Moreover, in this paper can be verified in Fig. 4(a–d), a dependence of the PL behavior, mainly with respect to its variation in emission intensities due to effect of different kind of surfactant (CTAB, PVP-40, and SDS) employed or without surfactant. Therefore, can attribute that these differences in the intensities of PL emissions of our β-$ZnMoO_4$ microcrystals are due to presence of changes in shape, crystal size, and surface defects.

An important point that can be verified is the broad profile of curve and proximity of maximum of PL emissions located in the range from 588 nm to 598 nm, i.e., yellow or orange regions of the visible electromagnetic spectrum. This characteristic is related to optical band gap values are very close between 3.1 and 3.25 eV. However, more detail on the electronic structure, excited states and PL properties of this molybdate will be the subject of further research. Recently, the literature has reported theoretical and experimental studies relevant to explain the electronic structure, surface energy and PL properties of some molybdates and tungstates [47–49]. In this communication, we have observed a highest emission for the microcrystals obtained with CTAB (Fig. 4(a) and Inset), while the lowest was verified for those synthesized with SDS (Fig. 4(d) and Inset). The irregular plates-like β-$ZnMoO_4$ microcrystals prepared without surfactant exhibited a considerable PL intensity with maximum emission at 590 nm near the same region of crystals prepared with CTAB surfactant (Fig. 4(b) and Inset). In addition, when compared to the other crystals, it was noted in

Fig. 4(c) that the fine plates-like β-$ZnMoO_4$ microcrystals prepared with the PVP-K40 surfactant presented an intermediate PL intensity (blue visible emission; Inset Fig. 4(c)). Analyzing these experimental results, we presume that these features are directly associated to the preferential orientation and/or structural defects (oxygen vacancies, distortion of chemical bonds) arising from imperfectly attached interfaces between the nanocrystals, crystal sizes and shapes. This conclusion can be supported by the XRD patterns data due to preferred orientation (Fig. 1(a–d)). Theoretically, the existence of defects are able to modulate the density of intermediary energy states within the forbidden band gap due to order–disorder effects and distortions on the octahedral $[ZnO_6]/[MoO_6]$ clusters, that affects the PL behavior.

4. Conclusions

In summary, β-$ZnMoO_4$ microcrystals were synthesized by the HT system at 140 °C for 8 h without and with the surfactants (CTAB, PVP-K40, and SDS). Independent of surfactant, the XRD patterns indicate that the microcrystals obtained by this chemical route have a wolframite-type monoclinic structure with good degree of crystallinity. Another important point detected in these diffractograms was the existence of preferential orientation for the microcrystals prepared with SDS. As it was verified by means of FE-SEM images, the distinct surfactants changed the shape and average size of β-$ZnMoO_4$ microcrystals. It proved that the chemical nature of the surfactants (CTAB – cationic, SDS – anionic and PVP-K40 – non-ionic) differently acts between the Zn^{2+} and MoO_4^{2-} ions in solution, influencing in the formation and growth process of the microcrystals. The yellow, orange, and blue PL emission exhibited by these microcrystals at room temperature were attributed the different arrangements of intermediary energy levels within the forbidden band gap, as a consequence of preferred orientation and structural defects into the lattice.

Acknowledgments

The authors acknowledge the financial support of the Brazilian Research Financing Institutions: FAPESP (No. 2009/50303-4), CNPq and CAPES.

References

[1] S.C. Abrahams, J. Chem. Phys. 46 (1967) 2052–2063.
[2] W. Reichelt, T. Weber, T. Söhnel, S. Däbritz, Z. Anorg. Allg. Chem. 626 (2000) 2020–2027.
[3] K. Pavani, A. Ramanan, Eur. J. Inorg. Chem. 2005 (2005) 3080–3087.
[4] L.I. Ivleva, I.S. Voronina, L.Y. Berezovskaya, P.A. Lykov, V.V. Osiko, L.D. Iskhakova, Crystallogr. Rep. 53 (2008) 1087–1090.
[5] V.B. Mikhailik, H. Kraus, D. Wahl, H. Ehrenberg, M.S. Mykhaylyk, Nucl. Instrum. Method Phys. Res. A 526 (2006) 513–516.
[6] D. Spassky, A. Vasilev, I. Kamenskikh, V. Kolobanov, V. Mikhailin, A. Savon, L. Ivleva, I. Voronina, L. Berezovskaya, Phys. Status Solidi A 206 (2009) 1579–1583.
[7] A. Xei, X. Yuan, F. Wang, Y. Shi, Z. Mu, J. Phys. D: Appl. Phys. 43 (2010) 055101–055105.
[8] L. Yu, M. Nogami, Mater. Lett. 64 (2010) 1644–1646.
[9] X. Ju, X. Li, W. Li, W. Yang, C. Tao, Mater. Lett. 65 (2011) 2642–2644.
[10] Y. Li, G. Weisheng, B. Bo, G. Kaijie, IEEE Int. Conf. Energy Environ. Technol. 3 (2009) 672–675.
[11] C. Arnaboldi, C. Brofferio, O. Cremonesi, L. Gironi, M. Pavan, G. Pessina, S. Pirro, E. Previtali, Astropart. Phys. 34 (2011) 797–804.
[12] L. Gironi, C. Arnaboldi, J.W. Beeman, O. Cremonesi, F.A. Danevich, V.Y. Degoda, L.I. Ivleva, L.L. Nagornaya, M. Pavan, G. Pessina, S. Pirro, V.I. Tretyak, V.I. Tupitsyna, J. Instrum. 5 (2010) P11007–P11011.
[13] B.D. Amo, R. Ramagnoli, V.F. Vetetre, J. Appl. Electrochem. 29 (1999) 1401–1407.
[14] N.N. Leyzerovich, K.G. Bramnik, T. Buhrmester, H. Ehrenberg, H. Fuess, J. Power Sources 127 (2004) 76–84.
[15] A.M.E.S. Raj, C. Mallika, K. Swaminathan, O.M. Sreedharan, K.S. Nagaraja, Sens. Actuators B. Chem. 81 (2002) 229–236.
[16] N. Sotani, T. Suzuki, K. Nakamura, K. Eda, S. Hasegawa, J. Mater. Sci. 36 (2001) 703–713.
[17] M. Kurzawa, M. Bosacka, J. Therm. Anal. Calorim. 60 (2000) 177–181.
[18] A.L. Kruglyashov, E.M. Skou, Solid State Ionics 28 (1988) 233–236.
[19] A. Sen, P. Pramanik, Mater. Lett. 50 (2001) 287–294.
[20] C. Peng, L. Gao, S. Yang, J. Sun, Chem. Commun. 43 (2008) 5601–5603.
[21] J.H. Ryu, S.M. Koo, J.W. Yoon, C.S. Lim, K.B. Shim, Mater. Lett. 60 (2006) 1702–1705.
[22] G. Tian, S. Sun, Cryst. Res. Technol. 45 (2010) 188–194.
[23] Y.S. Cho, Y.D. Hun, Bull. Korean Chem. Soc. 32 (2011) 2087–2090.
[24] J.C. Sczancoski, M.D.R. Bomio, L.S. Cavalcante, M.R. Joya, P.S. Pizani, J.A. Varela, E. Longo, M. Siu Li, J.A. Andrés, J. Phys. Chem. C 113 (2009) 5812–5822.
[25] V.M. Longo, A.T. de Figueiredo, A.B. Campos, J.W.M. Espinisa, A.C. Hernandes, C.A. Taft, J.R. Sambrano, J.A. Varela, E. Longo, J. Phys. Chem. A 112 (2008) 8920–8928.
[26] V.M. Longo, L. Garcia, D.G. Stroppa, L.S. Cavalcante, M.O. Orlandi, A.J. Ramirez, E.R. Leite, J. Andres, A. Beltran, J.A. Varela, E. Longo, J. Phys. Chem. C 115 (2011) 20113–20119.
[27] M.L. Moreira, E.C. Paris, G.S. do Nascimento, V.M. Longo, J.R. Sambrano, V.R. Mastelaro, M.I.B. Bernardi, J. Andrés, J.A. Varela, E. Longo, Acta Mater. 57 (2009) 5174–5185.
[28] M.L. Moreira, D.P. Volanti, J. Andrés, P.J.R. Montes, M.E.G. Valério, J.A. Varela, E. Longo, Scr. Mater. 64 (2011) 118–121.
[29] L.R. Macario, M.L. Moreira, J. Andrés, E. Longo, CrystEngComm. 12 (2011) 3612–3619.
[30] F. Lei, B. Yan, H.H. Chen, Q. Zhang, J.T. Zhao, Cryst. Growth Des. 9 (2009) 3730–3736.
[31] G. Zhang, S. Yu, Y. Yang, W. Jiang, S. Zhang, B. Huang, J. Cryst. Growth 312 (2010) 1866–1874.
[32] X. Yan, Y. Cui, W. Qi, Y. Su, Y. Yang, Q. He, J.B. Li, Small 4 (2008) 1687–1693.
[33] J. Fei, Y. Cui, X. Yan, W. Qi, Y. Yang, K. Wang, J.B Li, Adv. Mater. 20 (2008) 452–456.
[34] J. Meullemeestre, E. Penigault, Bull. Soc. Chim. Fr. 10 (1972) 3669–3674.
[35] L.S. Cavalcante, J.C. Sczancoski, R.L. Tranquilin, J.A. Varela, E. Longo, M.O. Orlandi, Particuology 7 (2009) 353–362.
[36] M. Halder, Chem. Educ. 12 (2007) 33–36.
[37] X.Z. Li, B. Walker, A. Michaelides, PNAS 108 (2011) 6369–6373.
[38] J. Emsley, Chem. Soc. Rev. 9 (1980) 91–124.
[39] Y. Mi, Z. Huang, F. Hu, Y. Li, J. Jiang, J. Phys. Chem. C 113 (2009) 20795–20799.
[40] Y. Tian, B. Chen, H. Yu, R. Hua, X. Li, J. Sun, L. Cheng, H. Zhong, J. Zhang, Y. Zheng, T. Yu, L. Huang, J. Colloid Interface Sci. 360 (2011) 586–592.
[41] M.L. Moreira, J. Andrés, V.R. Mastelaro, J.A. Varela, E. Longo, CrystEngComm. 13 (2011) 5818–5824.
[42] W.S. Wang, L. Zhen, C.Y. Xu, W.Z. Shao, Cryst. Growth. Des. 9 (2009) 1558–1568.
[43] Z. Luo, H. Li, H. Shu, K. Wang, J. Xia, Y. Yan, Mater. Chem. Phys. 110 (2008) 17–20.
[44] W. Wang, Y. Hu, J. Goebl, Z. Lu, L. Zhen, Y. Yin, J. Phys. Chem. C 113 (2009) 16414–16423.
[45] V.S. Marques, L.S. Cavalcante, J.C. Sczancoski, A.F.P. Alcântara, M.O. Orlandi, E. Moraes, E. Longo, J.A. Varela, M.S. Li, M.R.M.C. Santos, Cryst. Growth. Des. 10 (2010) 4752–4768.
[46] V.M. Longo, L.S. Cavalcante, E.C. Paris, J.C. Sczancoski, P.S. Pizani, M.S. Li, J. Andrés, E. Longo, J.A. Varela, J. Phys. Chem. C 115 (2011) 5207–5219.
[47] J.C. Sczancoski, L.S. Cavalcante, N.L. Marana, R.O. da Silva, R.L. Tranquilin, M.R. Joya, P.S. Pizani, J.A. Varela, J.R. Sambrano, M. Siu Li, E. Longo, J. Andrés, Curr. Appl. Phys. 10 (2010) 614–624.
[48] L. Gracia, V.M. Longo, L.S. Cavalcante, A. Beltrán, W. Avansi, M.S. Li, V.R. Mastelaro, J.A. Varela, E. Longo, J. Andrés, J. Appl. Phys. 110 (2011) 043501–043511.
[49] L.S. Cavalcante, J.C. Sczancoski, R.L. Tranquilin, M.R. Joya, P.S. Pizani, J.A. Varela, E. Longo, J. Phys. Chem. Solids. 69 (2008) 2674–2680.